25. However, for the same $(t_{pc}/t_{d,l/2})$ variation as the top surface (6 to 16) the semi-infinite slab data on the bottom surface exceed the finite slab data by factors of 1.23 to 2.56 (23–156%). This indicates the influence of other variables, the time of phase-change at the opposite surface and the thickness of the wing.

The example heat-transfer coefficient distribution on the wing illustrates the necessity of using the numerical finite-slab data reduction procedure with the phase-change heat-transfer technique on mid-sections of thin fins and wings. However, the use of this method for calculating the actual heat-transfer coefficient distribution along a wing profile or phase-change isotherms is time consuming. Therefore, for practical engineering applications, a correlation of the results from this numerical digital computer program for the finite slab with heat exchange at both surfaces which will not be restricted to a given slab thickness or set of thermal physical properties is needed. Such a correlation has been obtained. This correlation is for fixed values of $\bar{T}_1$, $\bar{T}_2$ ($\bar{T}_1$ not necessarily equal to $\bar{T}_2$), and the temperature potential ratio $(T_{aw} - T_i)_1/(T_{aw} - T_i)_2$. It presents h/h_{sis} for surface 1 as a function of $(t_{pc,1}/t_{d,l/2})$ for surface 1 and contains lines for various constant values of the correlating parameter that specifies the time at which the phase-change occurs at surface 2 $(t_{pc,2}/t_{d,l/2})$. The correction factor (h/h_{sis}) for surface 2 is obtained from the correlation given for the reverse set of $\bar{T}$'s and the inverse temperature potential ratio matched in determining the correction factor for surface 1. In this situation, surface 2 is treated as if it were surface 1 and vice-versa. Thus it is possible to obtain a finite slab correction factor h/h_{sis} to the semi-infinite slab data reduction procedure used with the phase-change heat-transfer technique. This correction factor is a function of $t_{pc,1}/t_{d,l/2}$, $t_{pc,2}/t_{d,l/2}$, $\bar{T}_1$, $\bar{T}_2$, and $(T_{aw} - T_i)_1/(T_{aw} - T_i)_2$.

Summary of Results

A numerical digital computer program has been developed to calculate the heat-transfer coefficient to both sides of a finite, one-dimensional slab subject to the boundary condition ascribed to the phase-change coating heat transfer technique. A summary of results obtained from this program follows.

1) In a typical tunnel test situation where a thin wing was exposed to heating on both sides, the semi-infinite slab data reduction procedures gave heat-transfer coefficients as much as 375% too high on the side with the lowest heating. The error at the opposite-surface position where the level of heating was approximately five times higher was 29%. The thickness of the wing where these errors apply was 0.0656 in. ($t_{d,l/2} \approx 0.36$ sec).

2) The results from the finite-slab procedure have been correlated in the form of correction factors to the semi-infinite slab solution in terms of parameters normally used with the phase-change heat-transfer technique. These correlations are a) not restricted to slab thickness of thermophysical properties and b) easily used to obtain accurate data on thin model sections.

References

[1] Jones, R. A. and Hunt, J. L., "Use of Feasible Temperature Indicators for Obtaining Quantitative Aerodynamic Heat-Transfer Data," TR R-230, 1966, NASA.

[2] Garrett, L. B. and Pitts, J. I., "A General Transient Heat-Transfer Computer Program for Thermally Thick Walls," TM X-2058, 1970, NASA.

[3] Carslaw, H. S. and Jaeger, J. C., *Conduction of Heat in Solids*, 2nd ed., Oxford University Press, 1959.

[4] Scarborough, J. B., *Numerical Mathematical Analysis*, The Johns Hopkins Press, 1962, pp. 199–222.

[5] Connor, L. E., Sparks, V. W., and Bhadsanle, A. G., "Heat Transfer Tests of the NASA-MSC Space Shuttle Configuration at the Langley Research Center Mach 8 Variable Density Facility," LMSC/HREC D162761, Dec. 1970, Lockheed Missiles and Space Co., Huntsville, Ala.

Water and Oxygen Particles in Space from Apollo Missions

Ravi D. Sharma,* M. L. Kratage,† and A. C. Buffalano‡

Bellcomm, Washington, D. C.

Introduction

THE behavior of particulate and gaseous matter ejected from spacecraft is of considerable importance since such ejecta may contaminate critical optical surfaces and interfere with scientific observations. During several of the Apollo missions, photographic and visual data have been obtained showing releases of liquid H_2O, O_2 and H_2 in space. We have developed the necessary theoretical models describing the diffusion and lifetimes of such particulate clouds in space. This Note reviews the optical data, briefly refers to the physical models, and identifies their applicability to O_2 and H_2O data.

Review of Optical Data

During the Apollo lunar missions, the S-IVB rocket stage vents liquid O_2 and H_2 after the translunar injection burn. In addition, the Command and Service Module (CSM) periodically vents waste H_2O into space. A considerable amount of photographic data has been collected during these events by the Smithsonian Astrophysical Observatory (SAO) worldwide network of Baker Nunn satellite tracking stations.[1]

During the Apollo 8 mission the SAO station in Spain took a series of 150 photographs after the release of 3000 kg of oxygen from the S-IVB approximately 45,000 km from the Earth. One such frame is shown in Fig. 1. Light scattered from the solid O_2 particles indicates a fan-shaped cloud. The butterfly-shaped cloud is solid hydrogen which has been vented non-propulsively.

During the Apollo 9 mission, the S-IVB unexpectedly released a large cloud of oxygen at 100,000 km several hours

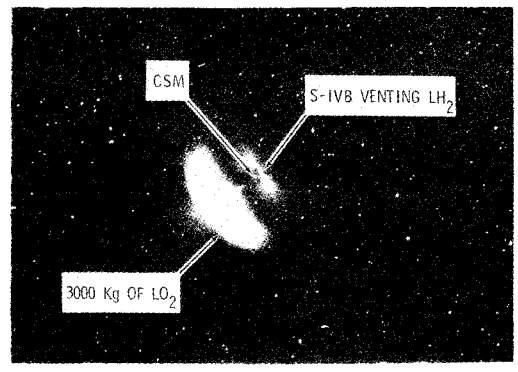

Fig. 1 Smithsonian Astrophysical Observatory photograph of Apollo 8 cryogen release.

Presented as Paper 71-474 at AIAA 6th Thermophysics Conference, Tullahoma, Tenn., April 26–28, 1971; submitted May 5, 1971, revision received August 16, 1971.

Index categories: Liquid and Solid Thermophysical Properties; Atmospheric Space and Oceanographic Sciences; Nozzle and Channel Flow.

* Member of the Technical Staff, Space Experiments Department.

† Associate Member of Technical Staff, Space Experiments Department.

‡ Former Member of the Technical Staff, Bellcomm; now an Aerospace Technologist, NASA Goddard Space Flight Center, Greenbelt, Md.

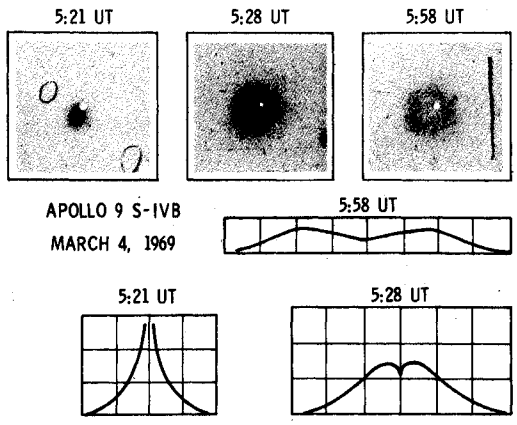

Fig. 2 Apollo 9 oxygen event photographs with corresponding density traces.

after its separation from the CSM and after its insertion into an escape orbit. The sequence of SAO frames showing this release, and schematic densitometric traces through the cloud at various times, is shown in Fig. 2. The cause of the release, which occurred several hours after the main liquid oxygen (LOX) dump, is unknown.

Apollo 12 photographs taken by the SAO have the diffused star images which will allow an absolute film calibration. Figure 3 shows a spherical H_2 cloud vented from the S-IVB before the LOX dump and the fan-shaped LOX cloud similar to the one in Fig. 1. Both were vented after the translunar injection. There was also a visual observation of a waste water release. Using a 24-in. Cassegrain telescope, J. Young of Table Mountain Observatory, Calif., observed the ice cloud formed by the water dumped from the spacecraft Environmental Control System. These data are summarized in Table 1. The dump began at 4:03 UT on Nov. 15, 1969 and lasted for 11 min during which 26.6 lb of water were released in space.

During the Apollo 13 mission, M. Charette and T. Troland of Amherst College Observatory used an 18-in. refractor to observe a waste water dump. The data are shown in Fig. 4. The dump began at 2:12 UT on April 12, 1970 and lasted for 10 min during which 23.4 lb of water were released in space. In these observations, the water cloud was described as an extended diffuse object like a nebula rather than as a point source like a star.

Physical Models

In our thermodynamic model,[2] we considered the energy balance among competing physical processes and found that the radii of particles decrease as $a = a_0 \exp(-t/\tau_s)$. For ice particles in cis-lunar space, τ_s is of the order of 1000 min. For O_2, assuming a small absorptive index, τ_s could be as large as 100 min. In fact, a lifetime of 100 min was calculated using the magnitude data from the oxygen clouds on Apollo 8. (Ref. 3).

Table 1 Apollo 12 water-dump data

Time from dump, min	Cloud Diameter		Visual magnitude (observed)	Range post flight, km
	Arc sec (observed)	km (calculated)		
15	5	2.68	12	106,200
20	10	5.35	12.5–13	106,800
29	15	8.00	13	107,400
33	20	10.70	14	108,300
51	30	16.00	15	111,400

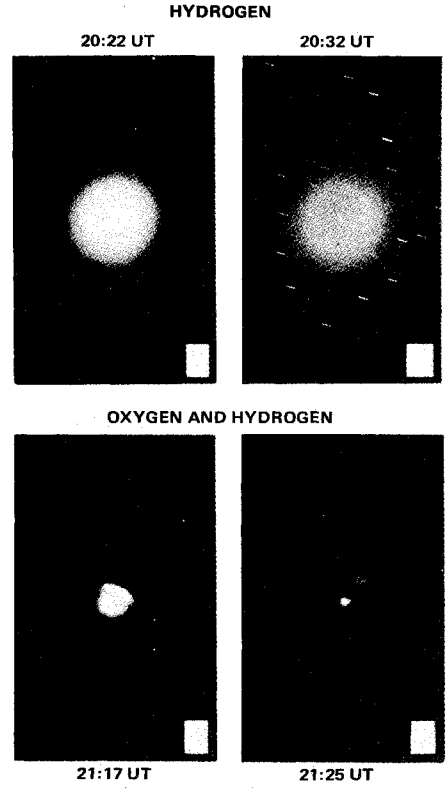

Fig. 3 Apollo 12 cryogen releases, Nov. 14, 1969.

In our dynamic model we studied two cases of expansion: 1) over a short period (~2 min) simulating the S-IVB oxygen blowdown,[3] and 2) over a longer period (~10 min) simulating the CSM waste water releases. The parameters giving a satisfactory fit (Fig. 5) to the Apollo 8 data are, in the notation of Ref. 3, $\theta_c = 30°$, bulk velocity $V_0 = 1.4 \times 10^4$ cm/sec and thermal velocity $V_t = 0.3 \times 10^4$ cm/sec.

Modeling the continuous waste water dumps is straightforward. We have assumed, based on the ratio of the heat of fusion to the heat of sublimation, that 15% of the liquid released must evaporate to freeze the rest. The number density of scatterers at a field point can be calculated by performing a convolution integration for the duration of the dump, τ_c, using the previous model[3] as the kernel. This gives the brightness at a field point, using the nomenclature in Ref. 3, as

$$\frac{B(r,t)}{B_\odot} = \left[\frac{3\Omega_\odot(0.85)}{(8\pi^{7/2}\rho_m a_0{}^3 V_t{}^3)}\right] \int_{-\infty}^{\infty} dl \int_0^{\tau_c} J d\tau \qquad (1)$$

where

$$J = (t-\tau)^{-3} Q(\tau)\sigma(\phi, t-\tau) H(t-\tau) \times \exp\{-V_t{}^{-2}[r/(t-\tau) - V_0]^2\}$$

The mass flow rate $Q(\tau)$ is assumed to be constant during the release.

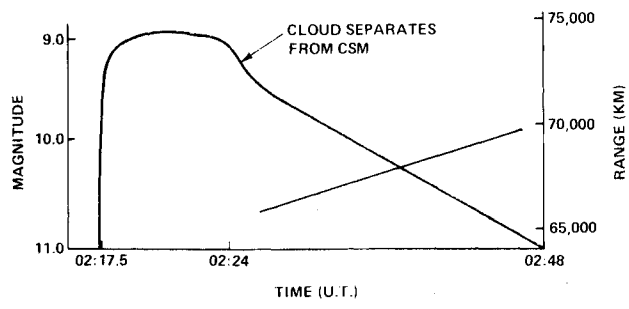

Fig. 4 Apollo 13 water dump data.

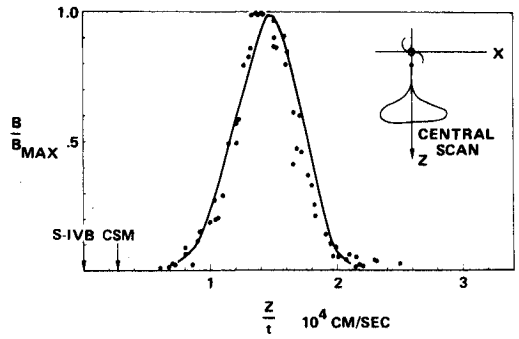

Fig. 5 Apollo oxygen data: relative brightness along a central scan.

The integration of brightness over the plane of the sky in Eq. (1) gives the magnitude of the cloud[3]

$$m(t) = m_\odot + 2.5 \log_{10}\{R^2(t)/\sigma_T(t)\} \qquad (2)$$

where $m_\odot$ is the solar magnitude, $R(t)$ is the range to the cloud and $\sigma_T(t)$ its total scattering cross section. Using Eq. (2), Table 1 and Fig. 4, the total scattering cross section can be calculated for each observation. These are shown in Fig. 6. We believe the clouds to be physically similar, and expect the scattering cross section of the cloud to be the same in both cases. Since the slopes are approximately the same, we conclude that while the observers could not fix a visual magnitude on the cloud, they were responding to changes in the appearance of the cloud in similar fashion.

If at time t_0 (20 min from initiation of the release) 85% of the material released consists of visible geometric scatterers of radius a_0, and if we use the mean value $\sigma_T(t_0) \approx 10^5$ cm^2 from Fig. 6, we obtain $a_0 = 750\ \mu$. This is consistent with observations of water dumps from inside the Apollo spacecraft.[4] Figure 6 also shows the changes in the cross section based upon sublimation alone, using the thermodynamic model. We see that sublimation alone cannot account for the observations.

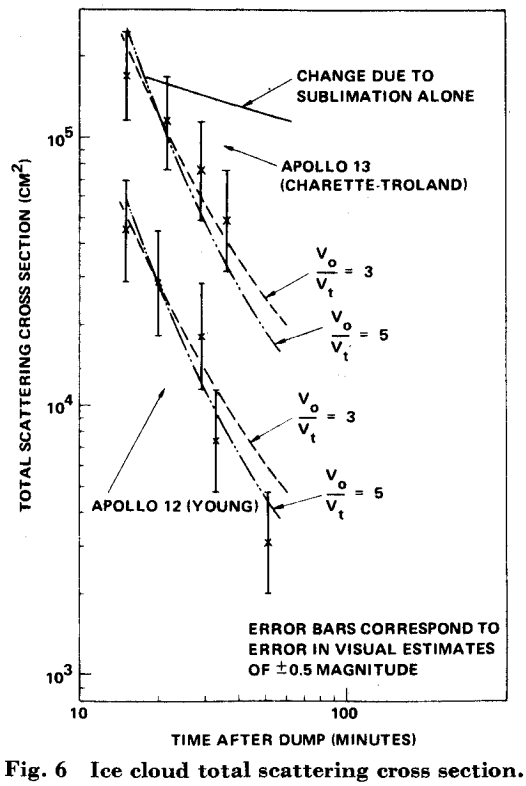

Fig. 6 Ice cloud total scattering cross section.

We tried to explain the reported magnitude and size data of the cloud using our continuous release model but could not obtain a consistent solution. However, if we assumed that the observers were responding to the peak brightness, $B_p(t)$, in the cloud, rather than to the magnitude, we found that the time dependence of $B_p(t)$ was the same as that of $\sigma_T(t)$. Thus we assumed $\sigma_T(t) = \sigma_T(t_0)\, B_p(t)/B_p(t_0)$.

The ratio of peak brightness at different times was calculated from the continuous release model using Eq. (1). We took the vent nozzle opening angle as 17° and the bulk velocity $V_0 = 600$ cm/sec (Ref. 5). The values of $\sigma_T(t)$ for $V_0/V_t = 3$ and $V_0/V_t = 5$, are plotted in Fig. 6. We see that the data are not sensitive to any detailed description; however, this ratio of bulk to thermal velocity is larger than unity and could easily be 5, as is the case for oxygen.

Thus, the best estimates for ice particles are $a_0 = 750\ \mu$, $\theta_c = 17°$ and $V_t \approx 120$–200 cm/sec. If the photographic observations of the cloud with diffuse star images were available, then a more detailed analysis would be possible.

References

[1] Lundquist, C. A., "Photometry from Apollo Tracking," *Space Research X*, North Holland Publishing Co., Amsterdam, 1970.

[2] Sharma, R. D. and Buffalano, A. C., "The Temperature and Size Histories of Liquid H_2, O_2 and H_2O Particles Released in Space," *Journal of Geophysical Research*, Vol. 76, Jan. 1, 1971, p. 232.

[3] Buffalano, C., "A Physical Model of Apollo Oxygen Release," *Journal of Geophysical Research*, Vol. 76, Jan. 1, 1971, p. 27.

[4] Kovar, R. P., "Light Scattering by Large Ice Particles," *Proceedings of the Symposium for Optical Contamination in Space*, Optical Society of America, 1969.

[5] Strelow, R. E., "Thrust Induced by ECS Fluids and Fuel Cell Purge Gases," Rept. IL-69S-322-110-68-058, North American Rockwell Corp., Downey, Calif.

Mass Blocking of Swirling Flow in Nozzles

CHENG-TING HSU
Iowa State University, Ames, Iowa

Introduction

A FEW years ago investigators were interested in determining the axial velocity distribution at the choking throat of a swirling-flow nozzle for the purpose of calculating the mass flow rate.[1–5] Results were controversial due to the assumptions made and the incorrect use of the flow equations. The purpose of this Note is: 1) to better understand the approximations and errors that were involved in previous works; and 2) to propose a concept of mass blocking of swirling flow in nozzles.

Review of Previous Works

All previous works discussed here concern a subsonic, isentropic, swirling flow through a convergent axisymmetric

Received June 1, 1971; revision received July 21, 1971. This research was supported by the Engineering Research Institute of Iowa State University.

Index category: Nozzle and Channel Flow.

* Professor, Department of Aerospace Engineering and Engineering Research Institute. Member AIAA.